Acta Crystallographica Section D
Biological Crystallography
ISSN 0907-4449

The binding of 2,4-dinitrophenol to wild-type and amyloidogenic transthyretin

Eurico Morais-de-Sá,[a]‡ Ricardo Miguel Neto-Silva,[a]‡ Pedro J. B. Pereira,[a] Maria J. Saraiva[a,b] and Ana M. Damas[a,b]*

[a]Instituto de Biologia Molecular e Celular–IBMC, Rua do Campo Alegre 823, 4150-180 Porto, Portugal, and [b]ICBAS, Universidade do Porto, Largo Prof. Abel Salazar 2, 4099-003 Porto, Portugal

‡ These authors contributed equally to this work and share first authorship.

Correspondence e-mail: amdamas@ibmc.up.pt

Received 11 January 2006
Accepted 25 February 2006

PDB References: TTR L55P–DNP, 2b14, r2b14sf; TTR-WT–DNP, 2b15, r2b15sf; TTR T78F–DNP, 2b16, r2b16sf.

Systemic deposition of transthyretin (TTR) amyloid fibrils is always observed in familial amyloidotic polyneuropathy, senile systemic amyloidosis and familial amyloidotic cardiomyopathy patients. Destabilization of the molecule leads to a cascade of events which result in fibril formation. The destabilization of a native protein with consequent conformational changes appears to be a common link in several human amyloid diseases. Intensive research has been directed towards finding small molecules that could work as therapeutic agents for the prevention/inhibition of amyloid diseases through stabilization of the native fold of the potentially amyloidogenic protein. This work provides insight into the structural determinants of the highly stabilizing effects of 2,4-dinitrophenol on wild-type TTR. It is also shown that similar interactions are established between this molecule and two highly amyloidogenic TTR variants: TTR L55P and TTR Y78F. In the three crystal complexes, 2,4-dinitrophenol occupies the two hormone-binding sites of the TTR tetramer. As a result of 2,4-dinitrophenol binding, the two dimers in the TTR tetramer become closer, increasing the stability of the protein. The three-dimensional structures now determined allow a comprehensive description of key interactions between transthyretin and 2,4-dinitrophenol, a small compound that holds promise as a template for the design of a therapeutical drug for amyloid diseases.

1. Introduction

Transthyretin (TTR) is a homotetrameric plasma protein that transports thyroid hormones, mainly thyroxine, and also retinol *via* interaction with the retinol-binding protein (Monaco *et al.*, 1995; Nilsson *et al.*, 1975). The crystal structure of TTR shows that each TTR monomer consists of a small helical fragment and eight β-strands, forming two β-sheets (DAGH and CBEF) that assemble as a β-sandwich structure (Blake *et al.*, 1978). The four identical subunits are arranged around a central channel that runs along the protein and in which the binding sites for two thyroxine molecules are located (Wojtczak *et al.*, 1996).

Familial amyloidotic polyneuropathy (FAP) and senile systemic amyloidosis (SSA) are neurodegenerative disorders that result from the aggregation of transthyretin into amyloid fibrils (Saraiva, 2001). The former is a hereditary form of amyloidosis caused by point mutations in TTR, whereas the latter is associated with wild-type TTR (TTR-WT) deposits, predominantly in the heart. Some TTR point mutations result in particularly aggressive forms of FAP and are therefore preferred targets for the investigation of strategies for therapeutic intervention. TTR L55P causes the most clinically aggressive FAP variant described so far (Jacobson *et al.*, 1992)

and biochemical data show that this protein has lower tetramer stability than the wild-type protein. The crystal structure of this variant was the first three-dimensional structure of TTR in which significant differences in relation to the wild-type protein could be observed, with the mutation resulting in the disruption of the hydrogen bonds between β-strands *D* and *A*, revealing new surfaces that may be involved in the aggregation process (Sebastião *et al.*, 1998). Interestingly, TTR L55P crystals were obtained from a solution that binds thioflavin-T, a fluorescent probe characteristic for an amyloidogenic fold (Sebastião *et al.*, 2000). A tyrosine to phenylalanine exchange at position 78 of the TTR amino-acid sequence leads to an amyloidogenic protein discovered for the first time in an Italian patient (Magy *et al.*, 2003). Its susceptibility to amyloid formation was studied *in vitro* and revealed a tendency to form amyloid fibrils comparable to that of the aggressive TTR L55P variant (Redondo *et al.*, 2000). Moreover, TTR Y78F is recognized in its soluble tetrameric form by a monoclonal antibody previously reported to react exclusively with highly amyloidogenic proteins that lack their native fold and with amyloid fibrils (Goldsteins *et al.*, 1999). Tyr78 belongs to the α-helical region of TTR and in the wild-type protein forms hydrogen bonds with Asp18 of the *AB* loop. X-ray crystallographic data showed that in the absence of this bond there is a destabilization of the contacts between the α-helix and *AB* loop and the body of the molecule, which may explain the highly amyloidogenic behaviour observed for this protein *in vitro* (Neto-Silva *et al.*, 2005).

At present, liver transplantation is the only available disease-stopping therapy for FAP patients (Lewis *et al.*, 1994). Despite the controversy regarding the nature of the building blocks of amyloid fibrils, dissociation of the tetramer is likely to be a crucial step in the mechanism of amyloid formation. In fact, several TTR variants associated with FAP have been shown to be less stable in the native tetrameric state than the wild-type protein (Damas *et al.*, 1996; Hammarstrom *et al.*, 2002; Quintas *et al.*, 1999). Thus, the discovery of small tetramer-stabilizing compounds for oral administration is gathering attention from researchers in this field. Presently, two drug classes, amyloid inhibitors and fibril disrupters, are being studied (Adamski-Werner *et al.*, 2004; Almeida *et al.*, 2004; Cardoso *et al.*, 2003; Green *et al.*, 2003; Klabunde *et al.*, 2000; Morais-de-Sá *et al.*, 2004). The former bind in the TTR central channel and stabilize the tetrameric structure by increasing the energetic barrier associated with tetramer dissociation, while the latter lead to the disruption of amyloid fibrils. Recently, a water-soluble molecule, 2,4-dinitrophenol (DNP), was shown to exhibit both inhibitory and fibril disruptor properties (Cardoso *et al.*, 2003; Raghu *et al.*, 2002) (Fig. 1). Furthermore, earlier studies suggested that DNP blocks the aggregation of the β-amyloid peptide and causes disruption of the fibrils associated with Alzheimer's disease (De Felice *et al.*, 2001). Taken together, these results suggest that DNP might be a starting point for the development of a common drug for the treatment of amyloid-related diseases.

In addition to its anti-amyloidogenic properties, DNP promotes neuritogenesis and neuronal differentiation, suggesting that it may also be used for developing therapeutic approaches in neurodegenerative pathologies (Wasilewska-Sampaio *et al.*, 2005).

In order to characterize at the molecular level the interactions of DNP with TTR-WT and two important mutants, TTR L55P and TTR Y78F, the three-dimensional structures of the three complexes were solved by X-ray crystallography.

2. Materials and methods

2.1. Protein complex preparation and crystallization

Solutions of DNP (Sigma, UK) at 25 mg ml^{-1} were prepared by dissolving the compound in DMSO. Purified TTR-WT, TTR Y78F and TTR L55P samples were dialyzed against 10 m*M* HEPES buffer pH 7.5 and concentrated to 16, 10 and 7.6 mg ml^{-1}, respectively. Each sample was incubated for one week at 277 K with a tenfold molar excess of DNP. The complexes were crystallized at 287 K by the hanging-drop vapour-diffusion method. The solution containing the complex was diluted 1:1 with reservoir solution. Crystals of the TTR-WT–DNP complex were grown using 2.0 *M* ammonium sulfate, 7% glycerol and 0.2 *M* sodium acetate pH 4.8 as precipitant. The TTR Y78F–DNP complex was crystallized with a reservoir solution consisting of 2.2 *M* ammonium sulfate, 7% glycerol and 0.2 *M* sodium acetate pH 5.4. Crystals of the TTR L55P–DNP complex were obtained using a reservoir solution containing 40% PEG 550 and 0.25 *M* HEPES pH 7.0. Under these conditions, crystals of the complexes were obtained after a few days. For each variant, one crystal was sequentially transferred to reservoir-like solutions with increasing concentrations of cryoprotectant

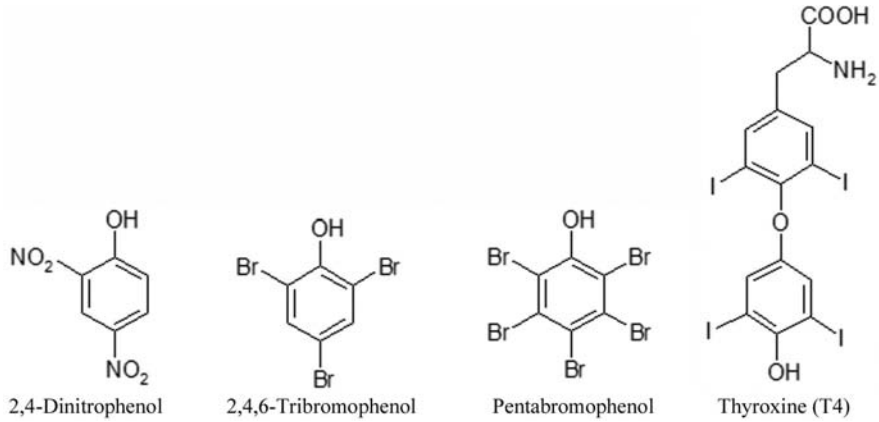

Figure 1
Schematic structures of 2,4-dinitrophenol (DNP), 2,4,6-tribromophenol, pentabromophenol and thyroxine, the natural ligand of TTR.

Table 1
Summary of data-collection and refinement statistics.

Values in parentheses are for the outermost resolution shell.

	TTR-WT–DNP	TTR T78F–DNP	TTR L55P–DNP
Crystallographic analysis			
Resolution range (Å)	35.54–1.7	32.67–1.75	50.85–2.0
Space group	$P2_12_12$	$P2_12_12$	$P2_12_12$
Unit-cell parameters (Å)	a = 42.6, b = 85.6, c = 63.9	a = 42.5, b = 85.9, c = 63.6	a = 42.5, b = 84.2, c = 63.4
No. of observations (total/unique)	93766/25884	123848/23470	95450/16093
Multiplicity	3.6 (3.6)	5.3 (4.8)	5.9 (5.6)
$R_{\rm merge}$†	8.3 (21.2)	6.1 (23.1)	6.6 (16.2)
Completeness (%)	98.5 (98.6)	97.8 (96.8)	99.1 (93.7)
$I/\sigma(I)$	5.0 (3.9)	8.4 (3.6)	6.5 (4.2)
Matthews coefficient (Å^3 Da^{-1})	2.14	2.22	2.28
Solvent content (%)	42.2	44.2	45.5
Structure refinement			
R factor‡/$R_{\rm free}$§ (%)	19.0/21.8	19.0/23.6	20.3/23.9
No. of unique reflections (working/test set)	24530/1319	22154/1196	15022/793
Water molecules	175	154	72
Ions	2 sulfates	—	—
Residues with alternate conformations (A and B refer to different monomers in the asymmetric unit)	Ser23*A*, Glu72*A*, Ser85*A*, Ser115*A*, Ser117*A*, Ser115*B*, Ser117*B*	Ser23*A*, Ser115*A*, Ser117*A*, Ser23*B*, Ser115*B*, Ser117*B*	—
Total No. of atoms	1941	1869	1783
No. of protein atom sites	1730	1689	1685
Average overall B factor (Å^2)	16.4	17.7	25.5
Average protein B factor (Å^2)	14.8	16.3	25.2
Average main-chain B factor (Å^2)	14.1	15.5	24.6
Average side-chain B factor (Å^2)	15.5	17.2	25.9
Average water B factor (Å^2)	30.4	31.9	31.3
Average ligand B factor (Å^2)	22.4	27.4	31.1
R.m.s. bonded B factors (Å^2)	1.278	1.424	1.424
R.m.s. deviations from ideal values			
Bonds (Å)	0.009	0.010	0.015
Angles (°)	1.2	1.3	1.6
Ramachandran plot statistics			
Most favoured region (%)	92	92	89.3
Additionally allowed region (%)	8.0	8.0	10.7

† $R_{\rm merge} = \sum_h \sum_i |I_{hi} - \langle I_h\rangle| / \sum_h \sum_i \langle I_h\rangle$, where I_{hi} is the observed intensity of the ith measurement of reflection h, including symmetry-related reflections, and $\langle I_h\rangle$ is the mean intensity of the i observations of reflection h over all measurements of I_{hi}. ‡ R factor = $\sum ||F_o| - |F_c|| / \sum |F_o|$, where $|F_o|$ and $|F_c|$ are observed and calculated structure-factor amplitudes, respectively. § $R_{\rm free}$ is the cross-validation R factor computed for a randomly chosen subset of 5% of the total number of reflections which were not used during refinement.

(10–25% glycerol). The crystals were cryocooled in liquid nitrogen.

2.2. Data collection and processing

X-ray diffraction data were collected at 100 K from single crystals using synchrotron radiation at beamlines ID14-EH1 (λ = 0.934 Å; TTR-WT–DNP and TTR Y78F–DNP) and ID14-EH4 (λ = 0.9786 Å; TTR L55P–DNP) of the European Synchrotron Radiation Facility (ESRF, Grenoble, France). For each crystallographic data set, determination of the crystal orientation and integration of the reflections were performed with *MOSFLM* (Leslie, 1992) and the data were reduced with *SCALA* (Collaborative Computational Project, Number 4, 1994). Structure factors were derived from intensities using the program *TRUNCATE* (Collaborative Computational Project, Number 4, 1994). The crystals from all three TTR variants belong to space group $P2_12_12$. Data-collection statistics are presented in Table 1.

2.3. Structure solution

The structures of the three complexes were solved by molecular-replacement techniques with *AMoRe* (Navaza, 1994) using data from 15 to 3.5 Å resolution and the atomic coordinates of the human TTR T119M structure (PDB code 1f86; Sebastião *et al.*, 2001) as a search model with residues 119 (TTR-WT), 78 and 119 (TTR Y78F) or 55 and 119 (TTR L55P) truncated to alanine.

2.4. Model building and structure refinement

An initial step of rigid-body refinement carried out with *CNS* (Brünger *et al.*, 1998) improved the molecular-replacement solutions. This program was subsequently used for simulated annealing and positional and individual temperature-factor refinement of the model. Automated refinement was alternated with manual fitting of the model into the difference electron-density maps using the graphic program *TURBO-FRODO* (Roussel & Cambilleau, 1989). In each round of refinement, water molecules were placed manually at the positions of positive peaks (>3σ) in the

difference Fourier maps, provided that good hydrogen-bond geometry was possible. The computed σ_A-weighted $(2F_o - F_c)$ and $(F_o - F_c)$ electron-density maps clearly showed positive electron density corresponding to the DNP molecule in both hormone-binding sites of the TTR tetramer for each complex. The atomic coordinates of the molecule were obtained from the HIC-UP database (Kleywegt & Jones, 1998) and the model of the ligand was manually fitted into the density. The model of the complex was further refined with *REFMAC* (Winn *et al.*, 2001). Half-occupancy was given to the DNP molecule as it is located on the twofold crystallographic symmetry axis. At the end of the refinement, the ligand and its symmetry-related positions are in good agreement with the final difference electron-density maps. The programs *PROCHECK* (Laskowski *et al.*, 1993) and *WHAT_CHECK* (Hooft *et al.*, 1996) were used to assess the quality of the model. A summary of the refinement statistics is given in Table 1.

3. Results and discussion

3.1. The binding of DNP to TTR

All three complexes crystallized in space group $P2_12_12$ and the structures were refined to resolutions of 1.7 Å (R = 0.190/R_{free} = 0.218), 1.75 Å (R = 0.190/R_{free} = 0.236) and 2.0 Å (R = 0.203/R_{free} = 0.239) for TTR-WT–DNP, TTR Y78F–DNP and TTR L55P–DNP, respectively. A summary of the refinement statistics is given in Table 1.

The final models show well defined electron-density maps for residues 10–124, except for monomer *A* of TTR-WT–DNP and monomer *B* of TTR L55P–DNP, for which residues 10–125 and 10–123, respectively, were modelled.

The crystals have two monomers (*A* and *B*) per asymmetric unit, which associate to form a dimer. The association of two dimers related by a crystallographic twofold axis results in tetrameric TTR with twofold symmetry along the axis of the hormone-binding channel. Therefore, the central channel comprises two hormone-binding sites and each of them consists of a pair of symmetry-related monomers A/A' or B/B' (the prime specifies a symmetry-related monomer or residue). The two binding sites are structurally equivalent and encompass a hydrophilic region closest to the centre, followed by a hydrophobic region and the channel entrance, near the charged Lys15 and Glu54 residues.

The difference Fourier and electron-density maps of the TTR–DNP complexes revealed the positions of the ligand bound deep in the T4 binding channel (Fig. 2). Owing to the crystallographic twofold axis that runs along the channel, two symmetry-related positions for 2,4-DNP were observed in each binding site. Thus, the observed electron density for the 2,4-DNP molecule is an average of the two positions.

The structures of the complexes closely resemble the structures of each unbound variant. The pairwise r.m.s.d. values for the main-chain atoms are 0.40, 0.14 and 0.75 Å for TTR-WT and TTR-WT–DNP, for TTR Y78F and TTR Y78F–DNP and for TTR L55P and TTR L55P–DNP, respectively. Small changes resulting from the binding of DNP can be observed in the hormone-binding channel and will be analysed in detail. The determined structures of DNP in complex with two TTR variants allowed us to evaluate for the first time the structural effect of tetramer-stabilizing compounds on variant proteins.

3.2. Structural features of the complexes underlying protein stabilization

The crystallographic structure of human TTR in complex with T4 allowed the first detailed description of the hormone-binding sites (Wojtczak *et al.*, 1996), which comprise three symmetry-related pairs of halogen-binding pockets. The outer pocket, P1, is delimited by the side chains of Ala108, Thr106, Met13 and Lys15. The central pocket, P2, is primarily hydrophobic and is formed by the methyl and methylene groups of Leu110, Ala109, Lys15 and Leu17. The innermost pocket, P3, is located between the side chains of Ala108, Leu110, Ser117 and Thr119. Much like P2, its surface is mostly hydrophobic, with hydrophilic contributions from Ser115 O^{γ}, the main-chain carbonyl groups of Ser117, Thr118 and Ala108 and the main-chain NH groups of Thr119, Ala109 and Leu110.

DNP has been described as a potent inhibitor of amyloid formation *in vitro* (Raghu *et al.*, 2002). To gain insight into the structural features responsible for the inhibition of TTR fibril formation by DNP, we solved the three-dimensional structures of its complexes with three different TTR variants: the wild type and the two highly amyloidogenic mutants L55P and Y78F.

The electron density observed in the channel for the different TTR–DNP complexes indicates the presence of bound ligand in both binding domains. The two binding sites are equivalent and thus only one of them will be described subsequently. The dinitro-substituted phenyl ring binds deeply in the channel in a forward mode, with the hydroxyl group pointing to the centre of the tetramer (Fig. 2*a*). This differs from what was observed for TTR in complex with pentabromophenol (PBP; PDB code 1e4h) and 2,4,6-tribromophenol (TBP; PDB code 1e5a) (Figs. 1 and 3) (Ghosh *et al.*, 2000). These structures show the phenolic ring with the hydroxyl group directed towards the entry of the binding channel. Moreover, both ligands appear in planes approximately perpendicular to that described for T4 in the TTR–T4 complex and the hydroxyl group does not seem to play a major role in binding, the interaction being mostly mediated by the halogens (Ghosh *et al.*, 2000). However, our work shows that the hydroxyl group of DNP is responsible for important protein–ligand interactions (Figs. 2*b* and 2*c*). It is accommodated in a region flanked by the P3 and P3′ pockets, establishing hydrogen bonds with the side-chain hydroxyl groups of Ser117 and its symmetry-related residue, thereby allowing new dimer–dimer interactions which underlie the overall protein-stabilization effects afforded by DNP. The aromatic ring of DNP slots between residues Leu17 and Leu110 from each dimer and is involved in hydrophobic interactions with them. The 2-nitro group O atoms are

Table 2
Hydrogen-bonding distances between DNP and TTR atoms.

Distances are in Å. Distances for protein atoms in alternate conformations are presented in parentheses.

	TTR-WT–DNP		TTR L55P–DNP		TTR Y78F–DNP	
Interaction	*A*	*B*	*A*	*B*	*A*	*B*
DNP OH—Ser117 OH	2.8	2.7	2.6	2.8	2.8 (3.0)	2.8 (3.0)
DNP OH—Ser117 OH′	3.0	3.2	2.7	3.2	2.9 (3.3)	2.8 (3.3)
DNP O_21—Ser117 OH	2.7	3.0	2.8	3.1	2.4 (2.3)	2.9 (2.3)
DNP O_21—Thr118 N	3.3	3.2	3.1	3.1	3.4	3.2
DNP O_22—Leu110 N	3.6	2.8	3.2	2.8	3.6	3.3
DNP O_22—Ala109 N	3.4	3.2	3.3	3.4	3.4	3.4

hydrogen bonded to the main-chain NH groups of Ala109, Leu110 and Thr118; an additional hydrogen bond to the hydroxyl group of the Ser117 side chain is established by one of the O atoms (Fig. 2*c*). This complex hydrogen-bonding network explains in part the high affinity of the compound for TTR. In fact, *in vitro* DNP binds TTR with higher potency than the natural ligand thyroxine (Raghu *et al.*, 2002). DNP also induces conformational changes of a few TTR residues, some of which may also exert a stabilizing effect on the TTR tetramer. In the ligand-free structure, the side-chain hydroxyl groups of Ser117 and Thr119 point towards the cavity and are hydrogen bonded to a water molecule. In all three complexes the side chains of Ser117 of both monomers are rotated along their $C^{\alpha}-C^{\beta}$ bond, allowing the formation of a strong hydrogen bond between the hydroxyl group and the bound DNP (Fig. 2*c*). Importantly, in the wild-type protein the ligand-induced conformational changes not only allow energetically favourable interactions between the inhibitor and the protein, but may also contribute to stabilizing the tetramer, since an alternative conformation allows intersubunit hydrogen bonds between the Ser117 residues on adjacent subunits in the same dimer (Fig. 3). An equivalent extra intersubunit interaction was also described for the TTR T119M variant (Sebastião *et al.*, 2001), which is known to have a protective effect over the amyloidogenic V30M mutation, an effect which is likely to be mediated by a more stable native state. The side chain of Thr119 also displays a DNP-induced rotation that together with the conformational change described for Ser117 leads to a more hydrophobic P3 pocket. The new orientation of the side chain of Thr119 places its hydroxyl group within hydrogen-bonding distance of a water molecule that interacts with the main-chain carbonyl group of Asp19 of the symmetry-related monomer, thereby providing a new dimer–dimer interaction. Superposition of the three newly determined crystallographic TTR–DNP structures does not show significant differences in the side chains of the residues lining the binding sites and in the position of the ligand itself (Fig. 2*b*). There is only a minor difference for the TTR L55P–DNP structure, in which the ligand is positioned slightly deeper into the binding site defined by monomers *B*/*B*′. However, this appears to be compensated for by an equivalent slight displacement of Ser117 and Leu110, two residues that establish important interactions with the ligand, thereby ensuring optimal DNP binding (Fig. 2*b*). The role played by the 4-nitro group in the interactions established between the inhibitor and the protein is not as important as the role described above for the other substituents of the aromatic ring. Nevertheless, this group interacts with water

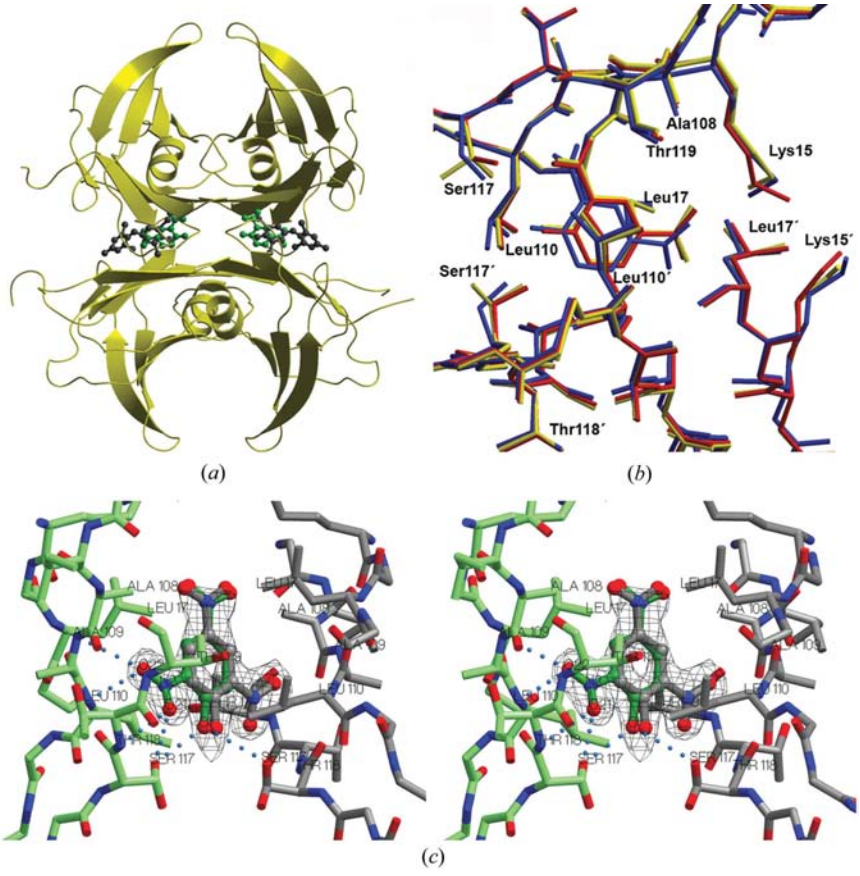

Figure 2
Interaction of DNP with TTR. (*a*) Localization of DNP (green) in the TTR hormone-binding channel. The thyroxine (grey) binding site is also shown. (*b*) Superposition of the DNP-binding site in the different human TTR variants. TTR-WT–DNP is depicted in yellow, TTR Y78F–DNP in red and TTR L55P–DNP in blue. The position occupied by DNP and by the protein atoms lining the binding channel is very similar in TTR-WT–DNP and in TTR Y78F–DNP, while in TTR L55P–DNP the DNP binds slightly deeper in monomer *B* and residues Leu110 and Ser117 are also slightly displaced towards the interior of the channel. (*c*) Detailed stereoview of the interactions established between DNP and WT-TTR. The two symmetric orientations of the DNP molecule in the binding site and the side chains of the protein residues that interact with the ligand are shown. Hydrogen bonds are represented as blue dashed lines. DNP is shown in ball-and-stick representation, with the initial $F_o - F_c$ electron-density map contoured at 2.5σ.

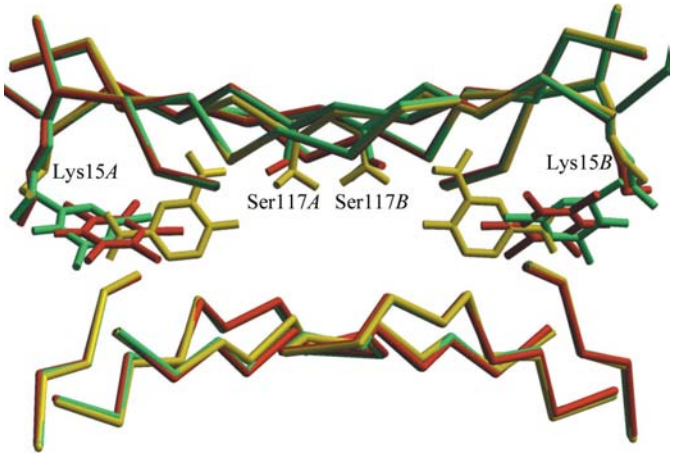

Figure 3
Superposition of the three-dimensional models of TTR-WT–DNP (yellow), TTR-WT–TBP (green; PDB code 1e5a) and TTR-WT–PBP (red; PDB code 1e4h). DNP binds deeper inside the central channel and its hydroxyl group establishes important interactions with Ser117. TBP and PBP bind to the protein in a plane approximately perpendicular to that described for T4 and the most important interactions are mediated by the halogen atoms with residues that line the entrance to the protein channel.

molecules located at the channel entry in all three complexes and may also contribute to the high affinity of the ligand for TTR by establishing van der Waals interactions with residues in the outermost part of the binding channel. A list of the most important hydrogen-bonding distances between DNP and the protein is presented in Table 2.

3.3. The orthorhombic structure of TTR L55P–DNP

The crystal structure of the TTR variant L55P was previously determined at 2.7 Å, revealing considerable differences from the wild-type protein and from other TTR variants (Sebastião *et al.*, 1998). It was the first TTR structure solved in space group *C*2, with one tetramer and two dimers per asymmetric unit (PDB code 5ttr). Recently, the crystal structure of a TTR complex with diethylstilbestrol (DES) was reported in the same monoclinic space group (Morais-de-Sá *et al.*, 2004).

The previously reported structure for TTR L55P revealed that the substitution of leucine by a proline, whose main-chain imino group cannot behave as a hydrogen-bond donor, results in the disruption of β-strand *D*. In fact, in the wild-type protein, only three hydrogen bonds link β-strand *D* to β-strand *A*. In the L55P variant reported here in space group $P2_12_12$ and at 2 Å resolution, the two hydrogen bonds that are established from the carbonyl O atom and amino group of residue 55 to the amino group and carbonyl O atom of Val14 are lost; however, the hydrogen bond established between the carbonyl O atom of Gly53 and the amino group of Val16 is maintained. The observed disruption of β-strand *D* argues against the proposal that different TTR pools may have different conformations owing to the high flexibility of strand *D* and that structures solved in space group $P2_12_12$ would not present a disrupted β-strand *D* (Hornberg *et al.*, 2004).

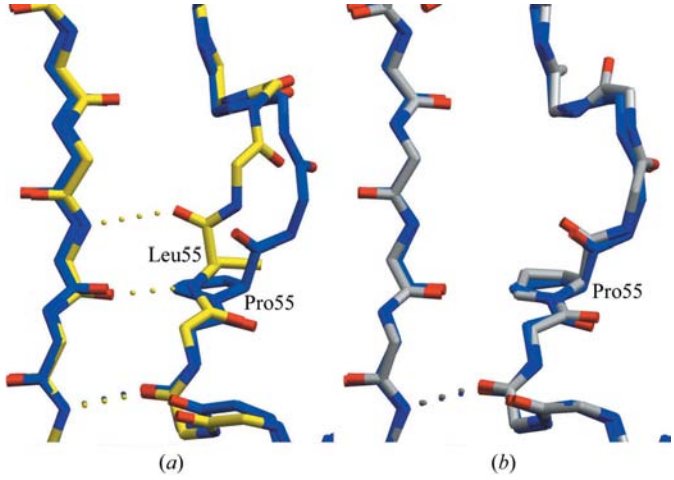

Figure 4
Main-chain superposition of residues 52–59 of TTR L55P–DNP (blue) and (*a*) TTR-WT–DNP (yellow) or (*b*) TTR L55P (grey; PDB code 5ttr). The β-strand *D* is disrupted in the orthorhombic L55P–DNP structure, which in this region displays a main-chain conformation nearly identical to that of the previously reported TTR L55P structure.

Moreover, the structure of the TTR–DES complex, which was solved in space group *C*2, displayed an intact β-strand *D*, indicating that the conformation of the strand *D* region does not directly correlate with the space group.

The conformation of the *D*-strand region in the orthorhombic TTR L55P–DNP complex is identical to that observed in the monoclinic TTR L55P structure, showing structural changes relative to the wild-type model in the folding of the region Pro55–Leu58 (Fig. 4). The major shifts in this region are for residues 55 and 56, whose C^{α} atoms are displaced by 1.6/1.7 and 2.3/2.8 Å (monomers *A*/*B*) when TTR L55P–DNP and TTR-WT–DNP are compared.

Thus, the crystal structure now reported shows that the structural modifications observed for strand *D* in TTR L55P are not space-group dependent; the presence of the disrupted β-strand *D* is probably related to the high susceptibility of this TTR variant to aggregation.

3.4. Polypeptide chain alterations induced by 2,4-dinitrophenol binding

In order to evaluate whether DNP binding had any effect on the overall protein structure, we used the method reported previously for extracting small differences in the TTR channel and binding sites (Neumann *et al.*, 2001; Wojtczak *et al.*, 2001). The difference in the distances between the C^{α} atoms of equivalent residues across the binding sites was determined for the distinct TTR variant complexes and their corresponding apo structures (WT, PDB codes 1tta; Y78F, 1x7s; L55P, 5ttr; Hamilton *et al.*, 1993; Neto-Silva *et al.*, 2005; Sebastião *et al.*, 1998). Apart from apo L55P, which contains a complete tetramer in the asymmetric unit, tetramers were generated by crystallographic symmetry and the $C^{\alpha}-C^{\alpha}$ distances between *A* and *A*′ and between *B* and *B*′ were measured. The data presented in Fig. 5 are the mean of the results obtained for the two binding sites, as no major differ-

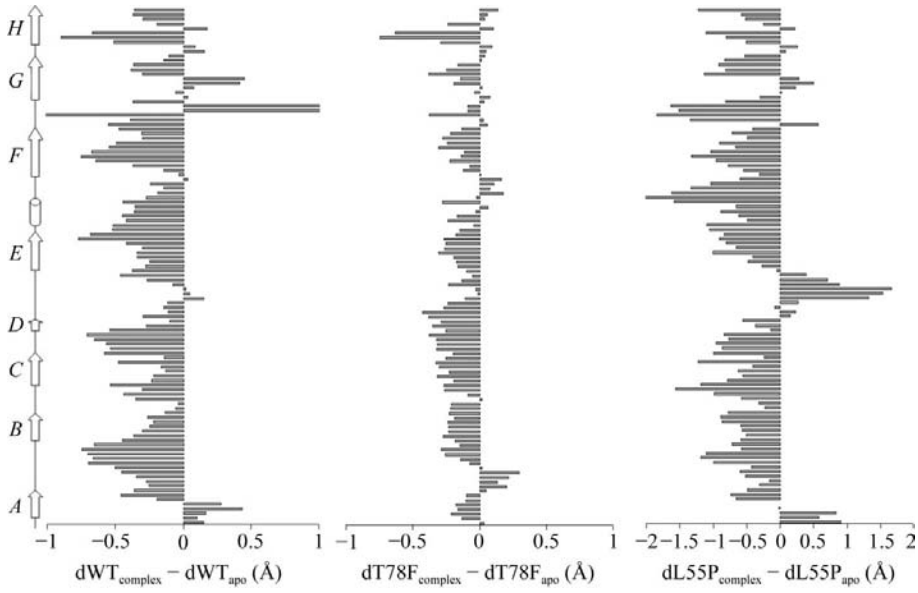

Figure 5
Protein backbone alterations induced by DNP binding. The differences between the distinct TTR–DNP complexes and the corresponding apo TTR variants are plotted for the $C^{\alpha}-C^{\alpha}$ distances measured across the TTR channel between equivalent amino acids (average across *AA′* and *BB′*).

ences were observed between them. In general, an evident reduction in the $C^{\alpha}-C^{\alpha}$ distance is noticeable for the three variants upon DNP binding. Interestingly, the largest variations in the backbone structure were observed for the L55P variant, which shows a collapse of more than 1 Å in the $C^{\alpha}-C^{\alpha}$ distance of several amino acids (note the different scale used in Fig. 5 for L55P). In this variant, there is a stretch of particularly high positive values that correspond to the $C^{\alpha}-C^{\alpha}$ distances for the residues that form the end of loop *DE*. The differences in crystal packing between our model and the previously solved monoclinic L55P structure justifies this irregularity, as this loop is involved in key contacts in the crystallographic packing of the monoclinic structure but not in the orthorhombic structures (Sebastião *et al.*, 1998).

The results obtained for the three variants indicate that DNP binding results in a more compact overall structure owing to an approximation of the amino acids that form the binding channel, which propagates to the rest of the TTR backbone. A general compaction of the protein structure leads to new van der Waals contacts, increasing protein stability. The same effect was previously reported for the binding of iodo-diflunisal and thyroxine to wild-type TTR (Gales *et al.*, 2005; Wojtczak *et al.*, 2001). Nonetheless, this is the first study showing at the structural level that drugs able to bind in the channel also stabilize highly amyloidogenic TTR variants responsible for the early onset of FAP.

4. Conclusions

In conclusion, this work unveils the structural determinants that underlie the stabilizing effects of DNP on TTR. This small compound establishes a set of hydrophobic and hydrophilic interactions with protein residues at the dimer–dimer interface which determine its deep localization in the hormone-binding channel, where ligand-induced conformational changes and new inter-subunit interactions are observed. For the first time, the interaction between a tetramer stabilizer and transthyretin variants is analysed at the molecular level. Furthermore, we present a high-resolution structure for the very aggressive L55P variant, which shows a significant shift of the *D* strand, confirming previous data obtained at lower resolution and in a different space group. Although the usefulness of DNP as an amyloid inhibitor *in vivo* remains to be addressed, the present study provides an important working platform that may prove valuable for the design of nitrophenol-based compounds to be used in the stabilization of potentially amyloidogenic human TTR variants.

This work was supported by grant POCTI/44821/2002 and by fellowships POCTI-PL180302-BI (EM-de-S) and POCTI-71999/NSE/35735 (RMNS) from Fundação para a Ciência e a Tecnologia, Portugal. The authors would like to thank Paul Moreira for excellent technical assistance in the preparation of recombinant transthyretin and acknowledge the European Synchrotron Radiation Facility for providing access to beamlines ID14-EH1 and ID14-EH4, and for the technical assistance given by the ESRF staff.

References

Adamski-Werner, S. L., Palaninathan, S. K., Sacchettini, J. C. & Kelly, J. W. (2004). *J. Med. Chem.* **47**, 355–374.
Almeida, M. R., Macedo, B., Cardoso, I., Alves, I., Valencia, G., Arsequell, G., Planas, A. & Saraiva, M. J. (2004). *Biochem. J.* **381**, 351–356.
Blake, C. C., Geisow, M. J., Oatley, S. J., Rerat, B. & Rerat, C. (1978). *J. Mol. Biol.* **121**, 339–356.
Brünger, A. T., Adams, P. D., Clore, G. M., DeLano, W. L., Gros, P., Grosse-Kunstleve, R. W., Jiang, J.-S., Kuszewski, J., Nilges, M., Pannu, N. S., Read, R. J., Rice, L. M., Simonson, T. & Warren, G. L. (1998). *Acta Cryst.* D**54**, 905–921.
Cardoso, I., Merlini, G. & Saraiva, M. J. (2003). *FASEB J.* **17**, 803–809.
Collaborative Computational Project, Number 4 (1994). *Acta Cryst.* D**50**, 760–763.
Damas, A. M., Ribeiro, S., Lamzin, V. S., Palha, J. A. & Saraiva, M. J. (1996). *Acta Cryst.* D**52**, 966–972.
De Felice, F. G., Houzel, J. C., Garcia-Abreu, J., Louzada, P. R. Jr, Afonso, R. C., Meirelles, M. N., Lent, R., Neto, V. M. & Ferreira, S. T. (2001). *FASEB J.* **15**, 1297–1299.
Gales, L., Macedo-Ribeiro, S., Arsequell, G., Valencia, G., Saraiva, M. J. & Damas, A. M. (2005). *Biochem. J.* **388**, 615–621.
Ghosh, M., Meerts, I. A., Cook, A., Bergman, A., Brouwer, A. & Johnson, L. N. (2000). *Acta Cryst.* D**56**, 1085–1095.
Goldsteins, G., Persson, H., Andersson, K., Olofsson, A., Dacklin, I., Edvinsson, A., Saraiva, M. J. & Lundgren, E. (1999). *Proc. Natl Acad. Sci. USA*, **96**, 3108–3113.

Green, N. S., Palaninathan, S. K., Sacchettini, J. C. & Kelly, J. W. (2003). *J. Am. Chem. Soc.* **125**, 13404–13414.
Hamilton, J. A., Steinrauf, L. K., Braden, B. C., Liepnieks, J., Benson, M. D., Holmgren, G., Sandgren, O. & Steen, L. (1993). *J. Biol. Chem.* **268**, 2416–2424.
Hammarstrom, P., Jiang, X., Hurshman, A. R., Powers, E. T. & Kelly, J. W. (2002). *Proc. Natl Acad. Sci. USA*, **99**, *Suppl.* 4, 16427–16432.
Hooft, R. W., Vriend, G., Sander, C. & Abola, E. E. (1996). *Nature (London)*, **381**, 272.
Hornberg, A., Olofsson, A., Eneqvist, T., Lundgren, E. & Sauer-Eriksson, A. E. (2004). *Biochim. Biophys. Acta*, **1700**, 93–104.
Jacobson, D. R., McFarlin, D. E., Kane, I. & Buxbaum, J. N. (1992). *Human Genet.* **89**, 353–356.
Klabunde, T., Petrassi, H. M., Oza, V. B., Raman, P., Kelly, J. W. & Sacchettini, J. C. (2000). *Nature Struct. Biol.* **7**, 312–321.
Kleywegt, G. J. & Jones, T. A. (1998). *Acta Cryst.* D**54**, 1119–1131.
Laskowski, R., MacArthur, M., Hutchinson, E. & Thornton, J. (1993). *J. Appl. Cryst.* **26**, 283–291.
Leslie, A. G. W. (1992). *Jnt CCP4/ESF–EACBM Newsl. Protein Crystallogr.* **26**.
Lewis, W. D., Skinner, M., Simms, R. W., Jones, L. A., Cohen, A. S. & Jenkins, R. L. (1994). *Clin. Transplant.* **8**, 107–110.
Magy, N., Liepnieks, J. J., Gil, H., Kantelip, B., Dupond, J. L., Kluve-Beckerman, B. & Benson, M. D. (2003). *Amyloid*, **10**, 29–33.
Monaco, H. L., Rizzi, M. & Coda, A. (1995). *Science*, **268**, 1039–1041.
Morais-de-Sá, E., Pereira, P. J. B., Saraiva, M. J. & Damas, A. M. (2004). *J. Biol. Chem.* **279**, 53483–53490.
Navaza, J. (1994). *Acta Cryst.* A**50**, 157–163.
Neto-Silva, R. M., Macedo-Ribeiro, S., Pereira, P. J. B., Coll, M., Saraiva, M. J. & Damas, A. M. (2005). *Acta Cryst.* D**61**, 333–339.
Neumann, P., Cody, V. & Wojtczak, A. (2001). *Acta Biochim. Pol.* **48**, 867–875.
Nilsson, S. F., Rask, L. & Peterson, P. A. (1975). *J. Biol. Chem.* **250**, 8554–8563.
Quintas, A., Saraiva, M. J. & Brito, R. M. (1999). *J. Biol. Chem.* **274**, 32943–32949.
Raghu, P., Reddy, G. B. & Sivakumar, B. (2002). *Arch. Biochem. Biophys.* **400**, 43–47.
Redondo, C., Damas, A. M., Olofsson, A., Lundgren, E. & Saraiva, M. J. (2000). *J. Mol. Biol.* **304**, 461–470.
Roussel, A. & Cambilleau, C. (1989). *Silicon Graphics Geometry Partners Directory*. Mountain View, CA, USA: Silicon Graphics.
Saraiva, M. J. (2001). *Hum. Mutat.* **17**, 493–503.
Sebastião, M. P., Lamzin, V., Saraiva, M. J. & Damas, A. M. (2001). *J. Mol. Biol.* **306**, 733–744.
Sebastião, M. P., Merlini, G., Saraiva, M. J. & Damas, A. M. (2000). *Biochem. J.* **351**, 273–279.
Sebastião, M. P., Saraiva, M. J. & Damas, A. M. (1998). *J. Biol. Chem.* **273**, 24715–24722.
Wasilewska-Sampaio, A. P., Silveira, M. S., Holub, O., Goecking, R., Gomes, F. C., Neto, V. M., Linden, R., Ferreira, S. T. & De Felice, F. G. (2005). *FASEB J.* **19**, 1627–1636.
Winn, M. D., Isupov, M. N. & Murshudov, G. N. (2001). *Acta Cryst.* D**57**, 122–133.
Wojtczak, A., Cody, V., Luft, J. R. & Pangborn, W. (1996). *Acta Cryst.* D**52**, 758–765.
Wojtczak, A., Neumann, P. & Cody, V. (2001). *Acta Cryst.* D**57**, 957–967.